World Journal of Engineering Research
ISSN: 2959-9873
DOI: https://doi.org/10.61784/wjer3012

SIMULATION ANALYSIS OF THE DYNAMIC RESPONSE CHARACTERISTICS OF A TYPICAL GOLD MINE TAILING DAM UNDER THE COUPLING OF EARTHQUAKE AND RAINFALL

PengJin Liu[1], Jie Wang[2], JiaFa Du[1], JianFei Sun[2*], YongLiang Zhang[2], HongWei Mu[2]
[1]*Qinghai Shanjin Mining Co. Ltd., Haixi 817000, Qinghai, China.*
[2]*School of Mechanical and Automotive Engineering, Qingdao University of Technology, Qingdao 266000, Shandong, China.*
Corresponding Author: JianFei Sun, Email: sunjianfei@qut.edu.cn

Abstract: When an earthquake and precipitation coincide, there is a considerable increase in the danger of tailing dam instability. This work chooses a typical metal mine tailing dam in the Jiaodong area and numerically models the danger of tailing dam instability under the coupling of earthquake and rainfall. The simulation is based on the genuine demand for efficient warning of tailing dam instability under extreme natural conditions. The analysis focuses on the tailing dam's displacement and instability risk in the event of a strong earthquake, intense rainfall, or a combination of the two. According to the simulation results, the middle and upper portions of the accumulation dam exhibit the largest horizontal displacement of the tailing dam, while the rainfall coupling condition exhibits the maximum horizontal displacement of the dam body. According to the study, there is a higher risk of dam failure in the upper-middle region of the tailing dam, and in two extremely harsh natural settings, an earthquake will have a more significant effect on the stability of the dam. The study's findings offer a solid scientific foundation for emergency planning and for monitoring and warning of tailing dams during severe natural disasters.
Keywords: Tailing dam; Rainfall and earthquake; Coupling action; Dynamic response

1 INTRODUCTION

One source of man-made debris flow hazards with a high potential energy is a tailings dam. Tailings dam failures have become more common in recent years[1]. The dam is vulnerable to a number of force sources during regular operation, and it is also susceptible to dam failure due to natural events like earthquakes and rainfall, which might have disastrous effects on the environment, property, and human lives. Consequently, it is crucial to research the integrity of tailings dams under extreme natural disturbances from a practical standpoint.

Many studies have been conducted on the stability of tailing dams from various angles, with a primary emphasis on seismic and rainy circumstances. Terzaghi and Michalowski used the proposed static force method to study seismic conditions [2-3], draw the slope stability diagram, and calculate the slope safety coefficient; In order to assess the tailing dam's dynamic stability, Haper and colleagues used the residual strength theory by using FLAC3D software [4]; Yasuda and colleagues conducted tests using a shaking table model [5], talked about the phenomena of residual deformation brought on by soil liquefaction, and suggested a technique for horizontal deformation prediction; In addition, Towhata and colleagues extended the mathematical equation for the lateral deformation of a laying liquefied soil layer and performed shaking table tests [6]; Seid-Karbasi M and others demonstrated that soil liquefaction significantly increases the risk of tailing dam instability [26]; R.S. Jakka and others investigated the stability of tailing dam constructed by upstream and downstream methods under different seismic wave conditions [4]. The study's findings demonstrated that the stability of tailing dam is affected by a variety of conditions, including the method of dam construction;Debarghya and colleagues simulated and examined the impact of soil liquefaction on the stability of tailing dams [3]; the findings demonstrated a considerable increase in the impact of soil liquefaction on tailing dam stability; Chakrabrabhan and others conducted numerical simulations of side slopes under seismic conditions [2], and explored the effect of different rock qualities and footings on the side slope stability; S. Srikrishnan and others carried out numerical simulations of side slopes under seismic conditions to investigate the effect of different rock qualities and footings on the slope stability [10]; B. Xu and colleagues used the limit equilibrium method to determine the tailing dam's liquefaction zone under dynamic loading conditions and came to the conclusion that the tailing dam was still stable under seismic conditions [11]; Strong earthquakes have a significant impact on the stability of tailings dams, according to research by Mahdi Naeini and others using SIGMA/W software to investigate the stress-pore pressure coupling of the dams under dynamic loading conditions [12]; Takaji used the Newmark method to determine whether seismic energy would cause slope landslides and to calculate the slope displacements following the occurrence of landslides [8].

Alonso and colleagues computed the two-site saturated seepage field in the rainy circumstances investigation [14], accounting for real fluctuations in air pressure; Sammori and others used the Galerkin method to analyze the factors affecting slope stability and deduced the temporary seepage state of the slope through experiments [15]. The study's

findings indicated that the infiltration coefficient, the slope's length, and the thickness of the soil layer all had an impact on the stability of the slope. Fledlund examined slope stability under heavy rainfall conditions and summarized the law of rainfall duration on the pore water pressure [16]; Muntohar conducted a study that determined the sliding time and damage depth of shallow slope instability brought on by rainfall [17]; Zandarín used a force-water coupled finite element model to simulate and analyze the dam [18], and the results indicated that the capillary phenomenon of capillary water had a significant impact on the dam's stability; Ormann conducted a finite element analysis of pore water pressure during the damming period [19], and the study showed that the stability of the tailing dam decreased with an increase in pore water pressure; N.G. and others simulated and examined the stability of rainfall slopes using finite element software [20]; Wang and others conducted experimental studies on tailing dam breaching under rainfall conditions, and generalized and summarized the increase in the length of the infiltration line with the increase in the length of the rainfall [21]. Tarek and others generalized the probability distribution function of the safety factor of the tailing dam by analyzing three factors: permeability coefficient, angle of internal friction, and cohesion [5]; An experimental research of tailings dam failure during rainfall was carried out by Wang and colleagues [21], who also described the changing rule of the infiltration line with the increase of rainfall duration; In experiments on hydraulic erosion on slopes subjected to rainfall, Sun and colleagues demonstrated that rainfall infiltration is the primary cause of the decline in slope stability [23]; Liu and others demonstrated that rainfall infiltration increases the tailing dam's pore water pressure [23], which impacts the stability of the dam; Rong Gui and others established a hydraulic deposition model to experimentally investigate the effects of rainfall infiltration on the stability of the dam [4].

The studies mentioned above primarily concentrate on the impact of a single factor on the stability of the tailing dam, rarely take into account the risk of instability of the tailing dam under extreme earthquake and rainfall coupling conditions, and do not offer recommendations for monitoring and warning of instability under such conditions. Based on this, tailing dam destabilization under high intensity earthquake, heavy rainfall, and the superposition of the two is studied through numerical simulation in order to reveal, study the risk of tailing dam destabilization under high intensity environments, and provide guidance on monitoring and warning of tailing dam destabilization as well as the creation of emergency response plans.

2 PROJECT OVERVIER AND MODEL CONSTRUCTION

2.1 Overview of the Project

In this study, a typical metal mine tailing dam in Jiaodong, Shandong province, is chosen for numerical simulation analysis. It is a valley-type tailing reservoir with a total capacity of 2.2455*106m3.In accordance with the Safety Technical Regulations for Tailing Reservoirs (AQ2006-2005), it is classified as a fourth-class tailing reservoir. With a slope ratio of 1:3, a maximum dam height of 12 meters, and a total storage capacity of 1.782 105 m3, the initial dam is a crushed rock-fill dam (Figure 1).

Figure 1 Tailing Dam Site

Strong earthquakes could happen in this location, according to studies of the regional geological structure and previous seismic data. The location falls within Group II of the Code for Seismic Design of Buildings (GB50011-2010), which has a seismic intensity of VII and a design fundamental seismic acceleration of 0.15g.

The yearly average for both temperature and precipitation is 11.8℃ and 637 mm, respectively. The rainy season typically begins in late June and lasts until early September. Precipitation at this time of year makes up around 75% of the total yearly amount and is characterized by intense, concentrated downpours with a maximum hourly precipitation of more than 50mm.

2.2 Model Construction and Boundary Condition Setting

FLAC3D software was selected for numerical simulation analysis in this paper because it can better handle the complicated subject of geotechnical bodies and can more intuitively demonstrate the emergence and development of large-model instability damage under complex multi-case settings. The more practical Rhino 7 program is utilized for modeling and meshing due to the intricacy of FLAC3D's built-in modeling. The model is then imported into FLAC3D for further study.

2.3 Modeling and Meshing

Based on the tailing dam's real dimensions—550 m for length, 300 m for breadth, and 100 m for height—a simplified model was created. The profile was segmented into seven areas based on the materials' mechanical and physical characteristics.

The Y-axis represents the vertical dam direction, the X-axis the direction along the dam strike, and the Z-axis the opposite direction of gravity. Figure 2 depicts the tailing dam's three-dimensional stability simulation model, which has 9466 zones and 6630 gridpoints.

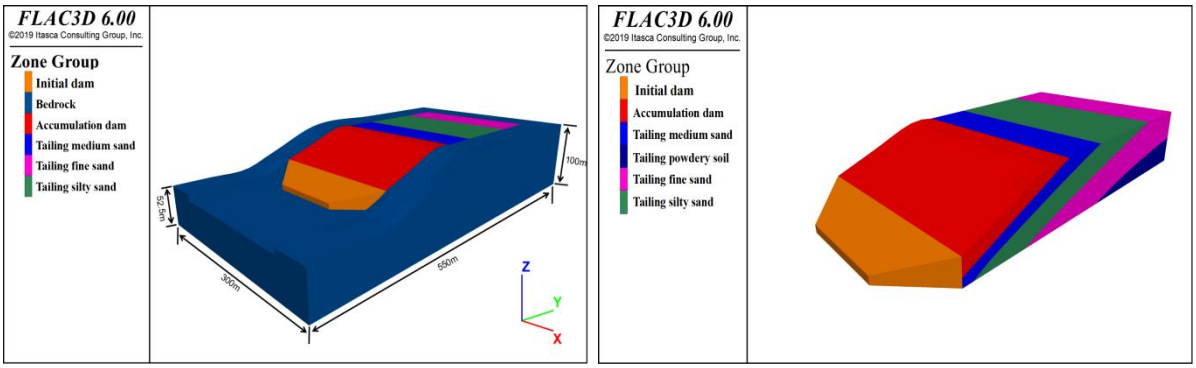

Figure 2 Numerical Calculation Model Diagram (Left: Numerical Modeling Diagram; Right: Reservoir Capacity Modeling Diagram)

2.4 Boundary Condition Setting

The bottom of the bedrock is subject to predetermined limits while defining the static field boundary conditions; the remaining direction is left free to tail in the tailing dam as a subsequent accumulation on the bedrock. The water table burial depth is set at eight meters in reference to the actual value of the engineering monitoring data.

In order to simulate the seismic condition, the static boundary condition is applied to the model's bedrock, the free boundary is placed around the model, and the static boundary condition is released to place the model in a free state.

The top plane of the reservoir area is designated as the permeable boundary, the bottom and two sides of the model are designated as the impermeable boundary, and the top plane is designated as the contact surface between rainwater and the dam body.

Determination of the intrinsic model and computational parameters:

The mohr-coulomb model was used for this tailing dam stability simulation because it primarily depicts loose and cemented granular bulk materials, and tailing sand has the properties of loose cementation. The density of the geotechnical body, the pertinent modulus of elasticity, the geotechnical body's strength characteristics, and poisson's ratio are the parameters that make up this model. The parameters used in the numerical simulation are all the values of the engineering field sampling experiment, which is shown in Table 1. The permeability coefficient in the table will also be used for numerical simulation of seepage during rainfall.

Table 1 Calculation Parameters

Ground Level	Density P(g/cm^3)	Friction Ψ(°)	Cohesion C(kPa)	Modulus of elasticity E(MPa)	Poisson	Permeability K(cm/s)
Tailing medium sand	1830	33	35	77	0.32	8.5×10-6
Tailing silty sand	1870	31	52	79	0.32	5.7×10-6
Tailing fine sand	1900	30	58	95	0.32	2.9×10-6
Tailing powdery soil	1940	29	65	110	0.32	1×10-6
Bedrock	2700	38	10000	10000	0.33	4.5×10-7
Initial dam	2400	36	1000	5000	0.33	6.5×10-7

Accumulation dam	1890	31	550	80	0.33	5.5×10-6

2.5 Input of Dynamic Loads

The "Code for Seismic Design of Buildings" (GB50011-2010) states that the tailing dam area's site characteristic period value is Tg = 0.30 s and the initial dam site's site characteristic period value is Tg = 0.40 s. These values are based on the project's building site category and the city's seismic grouping as group II.
Wenchuan wave is used in the simulation because the seismic intensity of the region where the tailing dam is located is grade VII. As a result, when the seismic wave is applied, the intensity of Wenchuan wave is adjusted to grade VII, and the corrected peak velocity is consistent with the peak velocity interval of grade VII earthquakes. As a result, the seismic wave can be used for the numerical simulation of subsequent grade VII earthquakes. Figure 3 depicts the seismic time curve following baseline correction. The earthquake lasted for a total of 16 seconds.

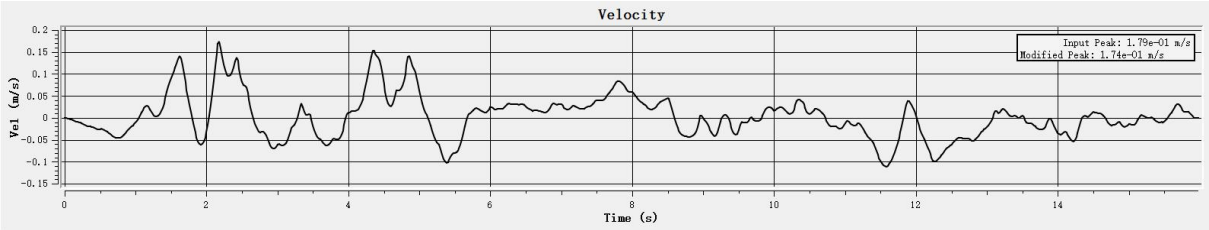

Figure 3 Seismic Velocity Time Course Profile after Filtering and Baseline Correction

2.6 Simulation Program

Stability simulations were created for the following four scenarios to examine the impacts of earthquake, rainfall, and their coupling on the stability of the tailing dam: 1) The static field condition; 2) The earthquake condition; 3) The rainfall condition; and 4) The coupling of the earthquake and rainfall.
Specific simulation programs are set up as follows:
(1) The initial total stress field, displacement field, and safety factor of the dam body are simulated in the static field condition with only the gravitational field applied, and the actual monitoring values are compared to make sure the ensuing simulation is accurate, which is of reference significance.
(2) Use the static method to determine the safety coefficient following an earthquake and the method of applying filtered and baseline-corrected ground vibration loads to the bottom of the tailing dam to determine the dynamic response of the dam body after the earthquake and perform the liquefaction analysis.
(3) To examine the dynamic reaction under the rainfall environment, a downpour with an imposed rainfall intensity of 50 mm/h is utilized, and the imposed time is 2, 4, 6, and 8 hours, respectively. This is done with reference to the actual rainfall in the local area.
(4) In the coupled case, a 16-second earthquake is applied first, followed by 50 mm/h rainstorms for 2, 4, 6, and 8 hours. This is done to investigate the dam's dynamic response to post-earthquake rainfall conditions as well as the distribution law of the dam instability region. This is because most earthquakes are accompanied by extended periods of heavy rainfall.

3 ANALYSIS OF SIMULATION RESULTS

Figure 4 depicts the Z direction total stress and pore-pressure cross section cloud of the tailing dam in the scenario where the gravity field is the only applied force.

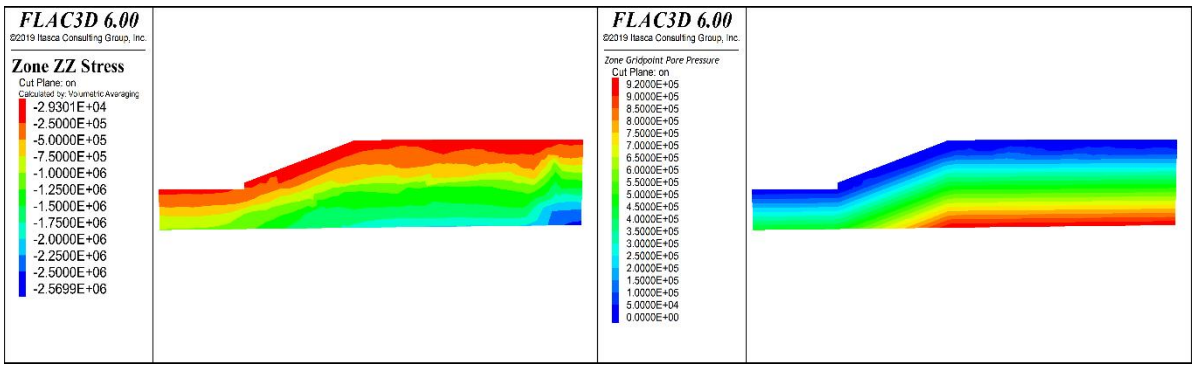

Figure 4 Total Stress and Pore-Pressure Cloud Diagram (Left: Z Direction Total Stress Cloud; Right: Initial Pore-Pressure Cloud)

The cloud map reveals:

(1) The maximum value of the total stress cloud map of the tailings dam is about 2.57MPa, and the maximum value of pore-pressure is 0.92Mpa, and their distribution pattern is basically the same. The maximum values are located at the bottom of the dam.
(2) Since the tailing dam's primary stress is compressive stress, as indicated by its total stress map, there won't be any visible tensile damage zone while the tailing dam is in a static field condition.
(3) Under static field conditions, the tailing dam's bottom region is where its maximum total stress is distributed. The distribution of the stress is essentially parallel to that of the terrain, which is consistent with the depositional properties of the soil body.

3.1 Displacement Field Analysis

Figure 5 depicts the displacement cloud in the Y-axis direction and the Z-axis direction when only the gravity field is used.

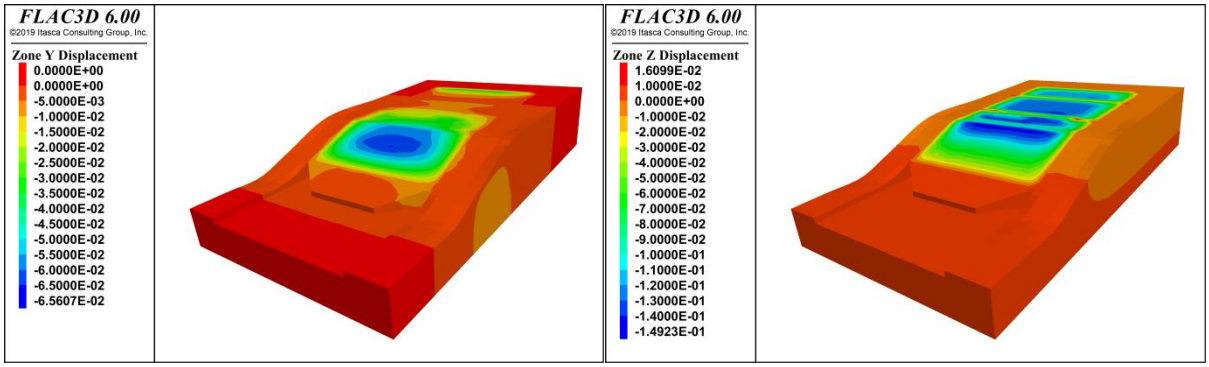

Figure 5 Overall Displacement Cloud (Left:Y-Axis Displacement Map; Right: Z-Axis Displacement Map)

The maximum displacement of the tailing dam in the vertical direction, which is shown in Fig. 5(Left), is concentrated in the middle of the tailing accumulation slope and is approximately 6.56 cm. The surface displacement of the reservoir area is also greater than the internal displacement of the reservoir area. This demonstrates that the displacement distribution pattern in the vertical dam direction is characterized by a surface displacement that is greater than an internal displacement. The accumulation dam's slope, where the biggest displacement is located, suggests that this area is less stable than others because of its lower stability.
According to Figure 5 (Right), the dry beach area and the accumulation slope are where the tailing dam's maximum displacement in the vertical direction, which is approximately 14.9 cm, is concentrated. Greater than the internal displacement of the reservoir area is the surface displacement of the reservoir area.
For the analysis of the displacement cloud, the cross-section at the center point (X=-150m) was further chosen, and the profile displacement cloud is presented in Figure 6:

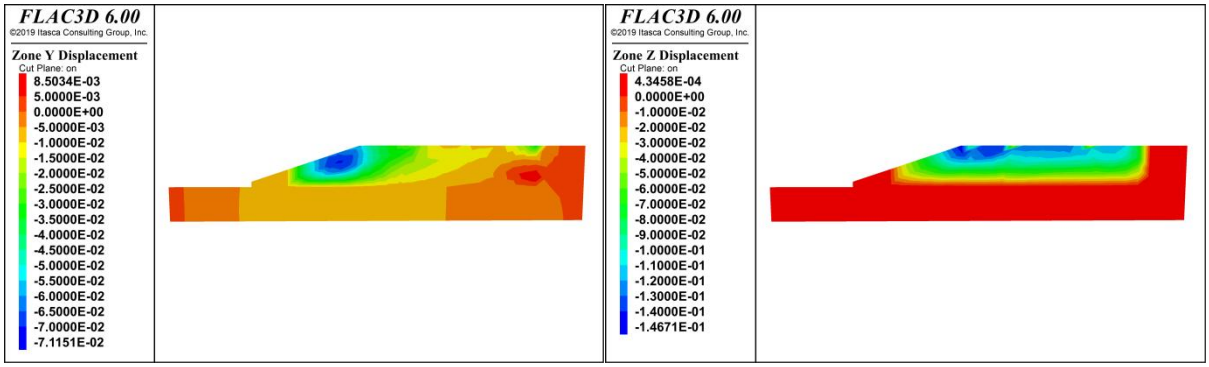

Figure 6 Displacement Cloud Map of the Profile(Left: Y-Axis Cross-Section Displacement Map; Right: Z-Axis Cross-Section Displacement Map)

As can be seen in Figure 6, the displacement distribution pattern in the Y-axis and Z-axis directions of the profile is the same as that of the whole, and the maximum displacement is concentrated on the slope surface and the top of the slope, and the displacement distribution shows the pattern of large surface and small internal displacement. In order to ensure that the simulation can truly characterize the actual displacement and instability, the simulation results were compared with the on-site displacement meter monitoring data, and the difference was in millimeters, which indicates that the model is in line with the actual site.

3.2 Three-Dimensional Dynamic Stability Calculation Results and Analysis

Stability analysis of dam under seismic conditions:

3.2.1 Displacement field analysis

The post-seismic displacement cloud of the tailing dam is shown in Figure 7:

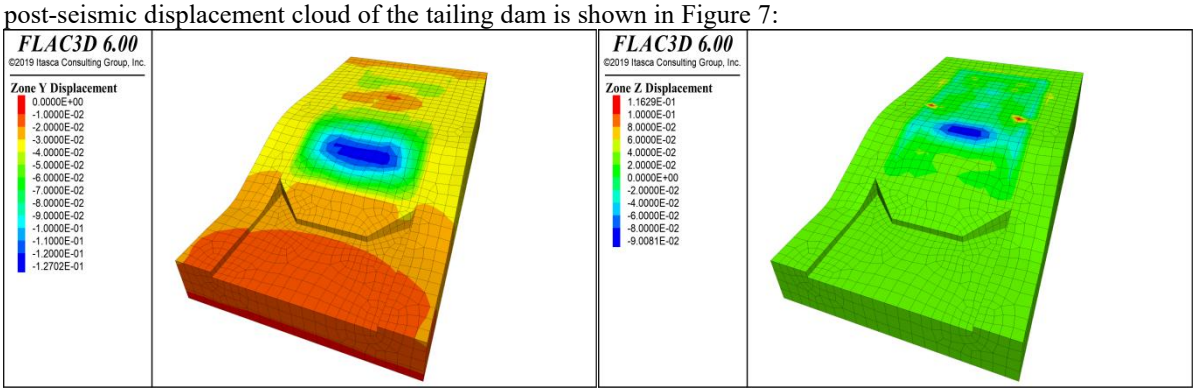

Figure 7 Overall Displacement(Left: Y-Axis Displacement Map; Right: Z-Axis Displacement Map)

The highest value of the tailing dam under seismic loading is shown in Figure 7 (Left), and it is approximately 12.7 cm in the vertical dam direction. The surface displacement of the reservoir area is also shown, and it is more than the internal displacement of the reservoir area. The initial dam's residual deformation is minimal, however the residual deformation of the accumulation dam and the dam body is substantial, showing that this position is less stable than other places.

Figure 7 (Right) illustrates that the highest vertical displacement of the tailing dam, which is approximately 9 cm, is located at the intersection of the dry beach and the stockpile slope.

Figure 8 depicts the displacement map of the profile, which was intercepted in the center of the pile slope (X=-150m) for analysis.

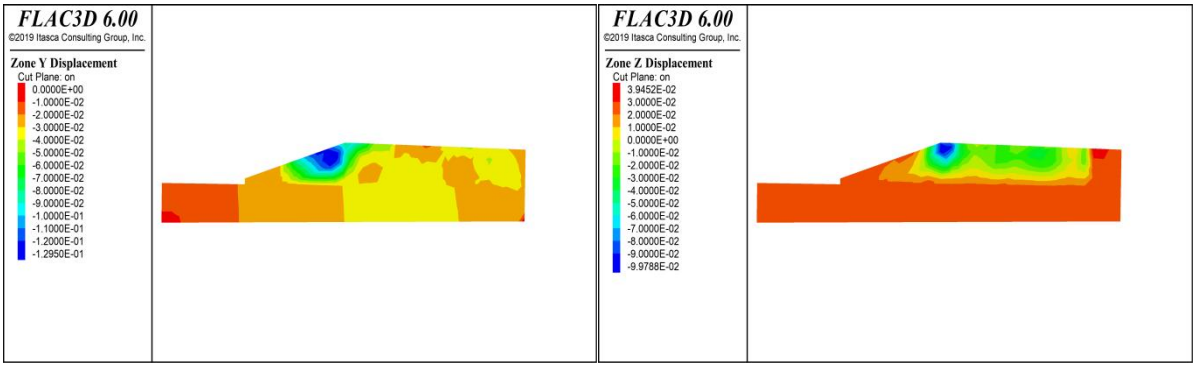

Figure 8 Cross-Sectional Displacement Cloud (Left: Y-Axis Cross-Section Displacement Cloud; Right: Z-Axis Cross-Section Displacement Cloud)

The maximum displacement is centered on the slope surface and the top of the pile-up slope, as seen in Figure 8. This distribution pattern of large surface and small interior is consistent with the only distribution pattern of the static field, and it further suggests that the middle-upper part of the pile-up slope is where the maximum displacement is distributed.

3.2.2 Judgment of liquefaction

(1) Judgment basis

In this study, we employ the excessive static pore-pressure ratio cloud diagram for liquefaction analysis, which is given the following definition by 3D numerical calculations(Yumin, 2013):

$$r_u = 1 - \frac{\sigma_1^{'}+\sigma_2^{'}+\sigma_3^{'}}{\sigma_{10}^{'}+\sigma_{20}^{'}+\sigma_{30}^{'}} \#(\text{Eq } 1) \quad (1)$$

$\sigma_{j0}^{'}(j = 1,2,3)$Three effective stress components of the unit before the dynamic calculation;

$\sigma_j^{'}(j = 1,2,3)$Three effective stress components of the cell during the dynamic calculation.

The magnitude of the degree of liquefaction can be determined by the super-porous pressure ratio, and its criteria are as follows: ru=1 denotes total liquefaction, and $0.7 \leqq ru<1$ denotes near liquefaction. In this study, we use fish language to write a program to calculate the excessive static pore-pressure ratio, generate the excessive static pore-pressure ratio cloud map, and then judge whether the tailings dam liquefaction.

(2) Liquefaction analysis of tailing dam

To ascertain whether soil liquefaction occurs in the reservoir region due to ground vibration load, the cloud diagram of super-porous pressure ratio in the reservoir area is examined. The cloud diagram of super-porous pressure ratio is illustrated in Figure 9:

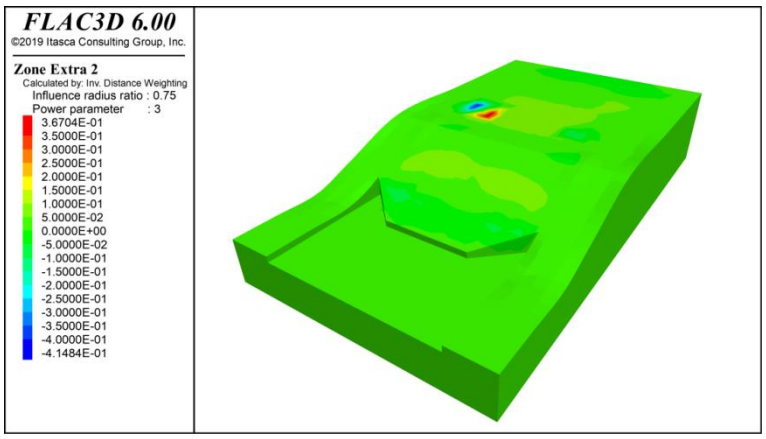

Figure 9 Cloud Diagram of Super-Porous Pressure Ratio

The tailing dam did not liquefy as a result of the earthquake, as can be seen from the study of the figure, which shows that the super-porous pressure ratios are minor after the earthquake and all locations are less than 0.7.

3.3 Dam Stability Analysis under Rainfall Conditions

The top of the tailings dam is selected as the precipitation infiltration surface, and the soil permeability coefficients of each layer are shown in Table 1 and Figure 10 displays the rainfall in the tailing dam displacement cloud maps at 2 hours, 4 hours, 6 hours, and 8 hours.

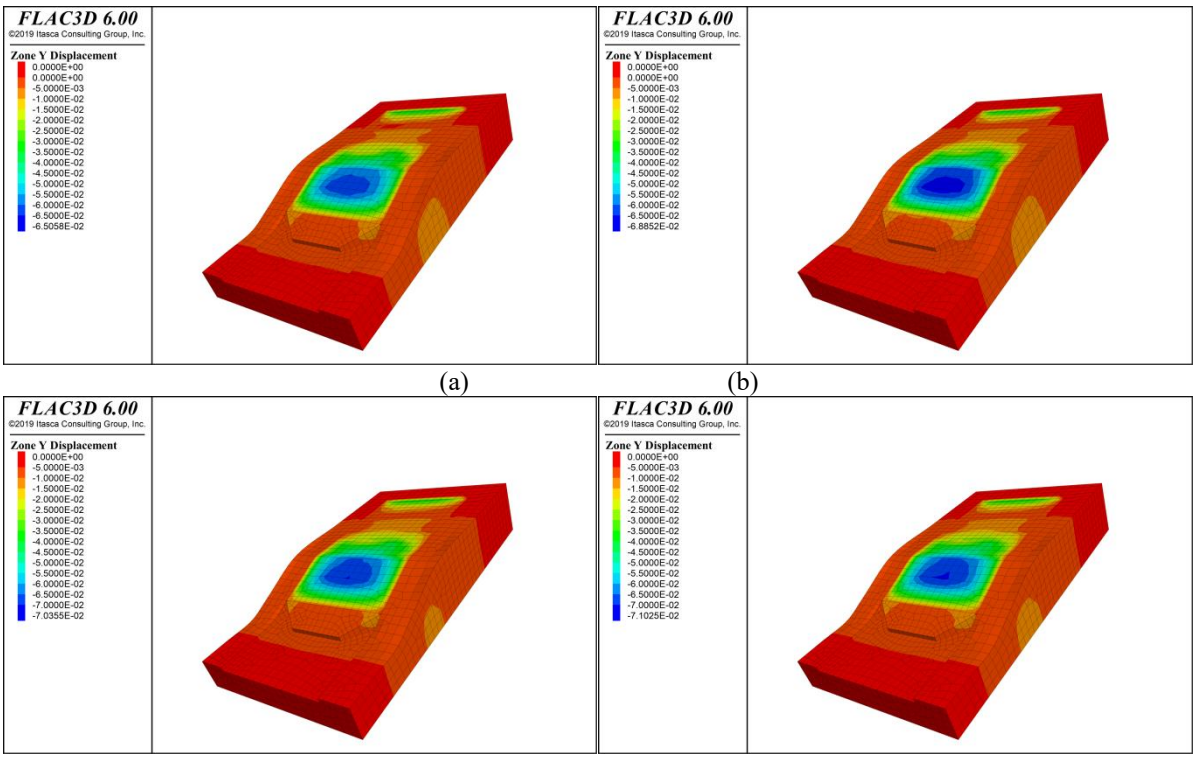

Figure 10 Displacement Cloud Map for Rainfall Condition (a: 2h Displacement Map; b: 4h Displacement Map; c: 6h Displacement Map; d: 8h Displacement Map)

Figure 10 illustrates how little the horizontal displacement of the dam body brought on by rainfall and how the overall stability of the dam body. The horizontal displacement of the dam body is distributed such that the deformation of the initial dam and reservoir area is small, the deformation of the accumulation dam is large, and the largest deformation area is concentrated in the accumulation dam slope and the top of the slope area, which is essentially the same as that of the deformation-prone area under the seismic condition. The amount of displacement with the increase of rainfall time also exhibits an increasing trend, i.e.

3.4 Stability Analysis of Dam under Coupled Conditions

In order to analyze the instability of the dam body under coupled seismic rainfall, the rainfall conditions are now overlaid on the seismic conditions, and the horizontal displacement distribution is illustrated in Figure 11:

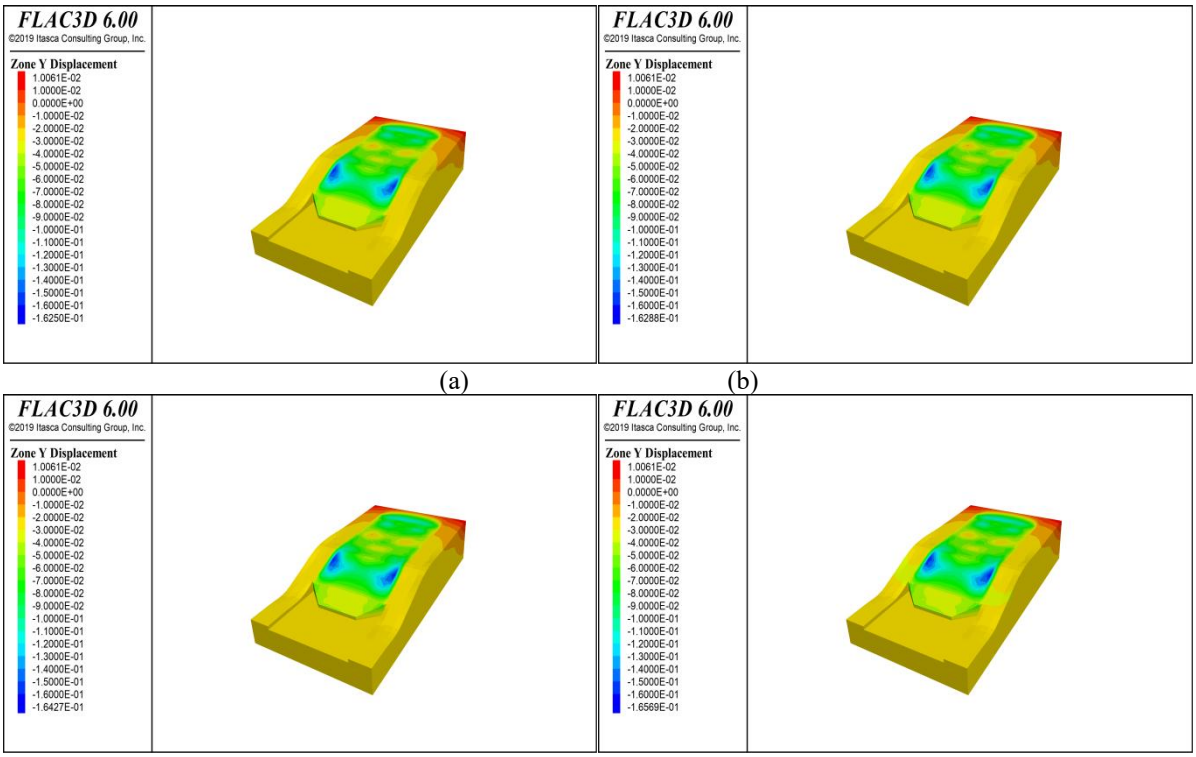

Figure 11 Horizontal Displacement Cloud for Coupling Condition (a: 2h Displacement Map; b: 4h Displacement Map; c: 6h Displacement Map; d: 8h Displacement Map)

According to the analysis of Figure 11, a large horizontal displacement of the dam body occurs when seismic rainfall coupling is present, but this displacement is distributed more unevenly for accumulation dam deformation than for initial dam and reservoir deformation.The stacking of the dam slopes and the rocky junction, as well as the lengthening of the rainfall period, are where the highest displacement is focused.The highest horizontal displacement exhibits an upward trend of around 16–17 cm, indicating that rainfall-earthquake coupling is present. The most severe damage to the stacked slopes was caused by the dam slope, demonstrating once more that the stability of the middle and upper regions of the dam slope is less stable than the reservoir in other locations and is susceptible to the characteristics of the phenomenon of extreme conditions of the dam collapse.

3.5 Dam Factor-of-Safety Analysis

The strength discount method was used to numerically simulate the safety factor of the dam body under the four operational circumstances; the simulation results are presented in Figure 12:

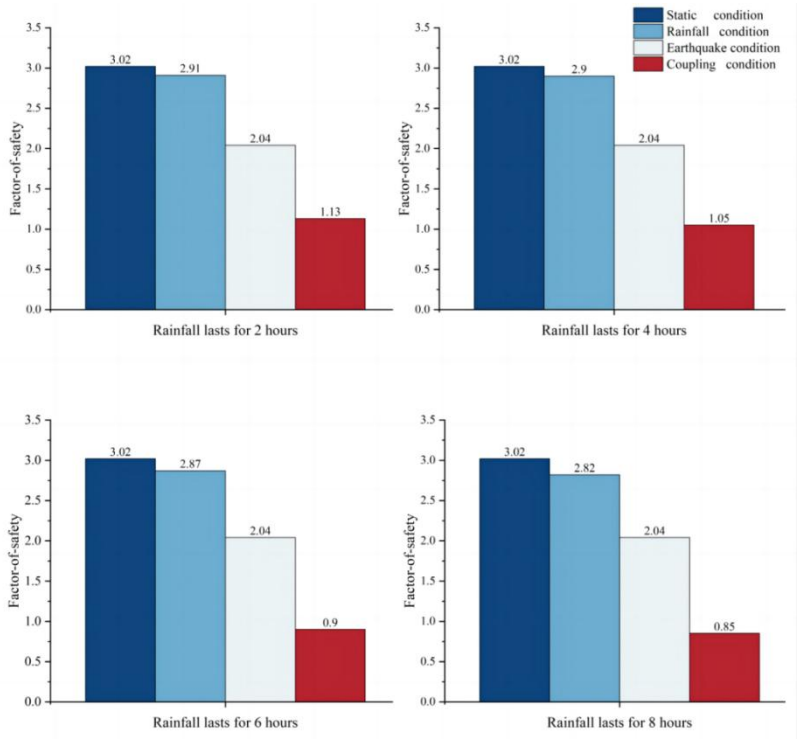

Figure 12 Tailing Dam Factor-of-Safety for Four Operating Conditions

Comparing the safety coefficients of tailing dams under the three working conditions, it can be seen that:
(1) The safety coefficient of the static field is 3.02, and the safety coefficient of the tailing dam following the earthquake is 2.04, both of which are greater than the minimum safety coefficients of 1.15 for normal operation and 1.00 for special operation of the fourth-class dam required by the Technical Specification for Geotechnical Engineering of tailing Impoundment dam (GB 50547-2010). Therefore, under the static condition and the VII magnitude earthquake condition, the tailing dam will remain stable.
(2) According to the Technical Specification for Geotechnical Engineering of tailing Impoundment Dam (GB 50547-2010), the overall safety factor of the tailing dam is greater than 2.8 under four rainfall duration, which is greater than the minimum safety factor of 1.05 under flood operation of the fourth class dam. As a result, the tailing dam can be operated safely even under eight hours of rain.
(3) The three extreme natural settings, which are rainfall and seismic environment, seismic environment, and rainfall environment in that order, will all have varying degrees of influence on the safety coefficient of the tailing dam. Among them, the short-term rainfall has less of an impact on the dam's safety factor, while the influence of earthquakes is significantly more than that of rainfall.
(4) When the rainfall duration is extended, the dam body safety coefficient falls even lower to below the critical value, increasing the risk of a dam failure. In the coupled condition, the dam body safety coefficient is 1.05 for 4 hours of continuous rainfall, approaching the specification's special operation critical value of 1.00.

3.6 Discussion on Risk of Destabilization and Warning

From the analysis of numerical simulation results, it can be seen:
(1) A strong earthquake, heavy rain, and a heavy rain Strong earthquake coupling under three conditions will affect the tailing dam's stability to varying degrees; the maximum deformation area's distribution varies slightly under each condition, but the horizontal displacement is primarily concentrated in the accumulation dam's slope area, and the displacement at the top of the slope is greater than the displacement at the foot of the slope, indicating that this area is the high-risk tailing dam instability. Under coupled conditions, the growth rate accelerates and the tailing dam's maximum horizontal displacement rises with the amount of rainfall. The safety coefficient in the coupled condition falls more than in the single influence factor condition, and in the coupled condition falls more than in the single rainfall condition when compared to the single seismic factor.
(2) The two extreme natural environments—heavy rainfall and a strong earthquake—have a significant impact on the maximum deformation of the dam body, which is approximately 6.56 cm and 12.9 cm, respectively. The strong earthquake causes a larger displacement of the dam body and increases its safety coefficient, making the stability of the dam body more vulnerable to seismic perturbation.
(3) According to the above study, more monitoring points should be placed close to the top of the tailing dam stockpile's slope when determining the sensor's location for the instability warning project in order to keep an eye on changes in the stockpile's displacement. The three parameters of earthquake intensity, precipitation intensity, and precipitation duration should be the main emphasis of the warning study. The tailing dam instability risk monitoring and

warning procedure under severe seismic downpour conditions is suggested based on the simulation results, as seen in Figure 13:

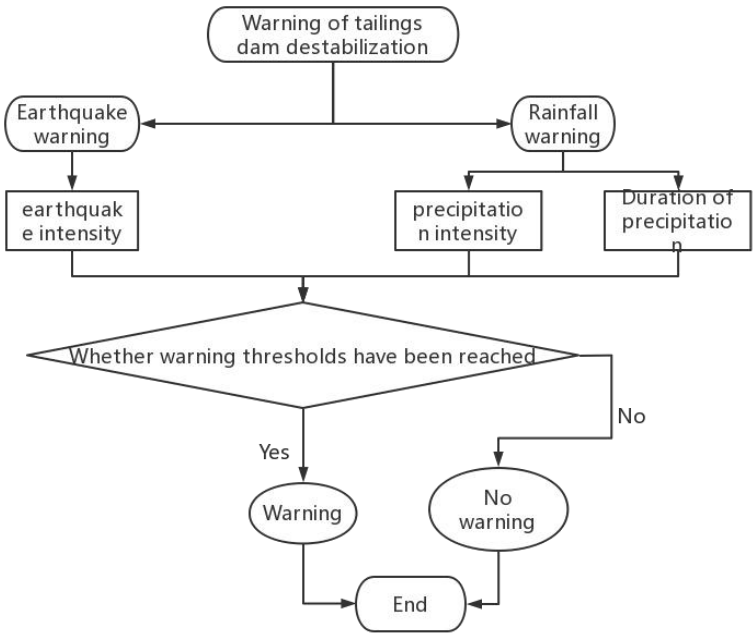

Figure 13 Flowchart for Monitoring and Alerting of Tailing Dam Instability in the Presence Of Seismic Rains in Extreme Circumstances

Among them:
(1) The simulation results indicate that the tailing dam can be operated safely under a magnitude VII earthquake, so the critical value of the seismic intensity warning for the tailing dam is set to VII. However, when it comes to applying this warning to other tailing dams, it should be adjusted based on the actual situation.
(2) In this investigation, the tailing dam can be operated safely under precipitation conditions of 50 mm/hr intensity and 8 hours of nonstop rain. Therefore, in the upcoming investigation, it is important to talk more about the warning thresholds for precipitation intensity and duration.
(3) In the coupling situation, the dam safety factor reached the critical value 4 hours after the VII earthquake due to precipitation at a rate of 50 mm/h, and this circumstance can be used to determine the warning critical value in this particular scenario.

4 CONCLUSION

(1) The stability of the tailing dam will be affected to varying degrees by the three extreme natural environments of earthquake, rainfall, and seismic rainfall. The maximum horizontal displacements in each of these conditions are 12.9 cm, 7.1 cm, and respectively. The maximum horizontal displacements are distributed in the middle and upper part of the slope of the accumulation dam, with a distribution pattern where the top of the slope is larger than the foot of the slope.
(2) The risk of dam failure arises from the safety coefficients of the dam gradually falling below the warning threshold after 4 hours in the coupled condition. The safety coefficients of the dam are 2.04, 2.80, and 0.85 in the three extreme natural environments of earthquake, rainfall, and seismic rainfall, respectively. The safety coefficient of the dam body is more affected by earthquakes than by heavy rainfall, and the stability of the dam body is more susceptible to seismic disturbance. Therefore, the design and operation of the tailing dam should prioritize enhancing the seismic performance of the dam body in addition to enhancing its drainage performance.
(3) In order to provide reference and guidance for the early warning study of the instability risk of tailing dam under extreme natural environments, the intensity and duration of the precipitation should be combined in the next study to investigate the precipitation warning critical value. Then, the earthquake should be superimposed to further investigate the early warning monitoring critical value of the tailing dam under the coupled conditions.

COMPETING INTERESTS

The authors have no relevant financial or non-financial interests to disclose.

DATA AVAILABLE STATEMENT

All data and models generated or used during the study appear in the submitted article

FUNDING

Thanks for the support of various funds for this study. The financial support for this study are as follows: (1) National Natural Science Foundation of China: Study on the mechanism of thermal-mass synergy effect on ventilation resistance under deep mining of metal ores (52374209, 52404222); (2) Natural Science Foundation of Shandong Province: Study on the mechanism of thermal-mass synergy effect on ventilation resistance under deep mining conditions in coastal metal mines (ZR2023ME012); (3) Natural Science Foundation of Shandong Province: Energy attenuation mechanism of excitation stress waves during coal-rock damage destabilization process (ZR2023QE080).

REFERENCES

[1] Wang K, Yang P, Yu G, et al. 3D Numerical Modelling of Tailings Dam Breach Run Out Flow over Complex Terrain: A Multidisciplinary Procedure. Water, 2020, 12(9): 2538. DOI: 10.3390/w12092538.

[2] Terzaghi K. Mechanism of landslides application of geology to engineering practice. Geol.Soc. America Berkley Volume, 2020, 65: 1950.

[3] Michalowski R, Asce F, Martel T, et al. Stability Charts for 3D Failures of Steep Slopes Subjected to Seismic Excitation. Journal of Geotechnical and Geoenvironmental Engineering, 2021, 137: 11-14. DOI: 10.1061/(ASCE)GT.1943-5606.0000412.

[4] Ishihara K (n.d.). Post-Earthquake Failure of a Tailings Dam Due to Liquefaction of Pond Deposit. 2011.

[5] Yasuda S, Nagase H, Kiku H, et al. The Mechanism and a Simplified Procedure for the Analysis of Permanent Ground Displacement Due to Liquefaction. Soils and Foundations, 1992, 32(1): 149–160. DOI: 10.3208/sandf1972.32.149.

[6] Towhata I, Sasaki Y, Tokida K-I, et al. Prediction of Permanent Displacement of Liquefied Ground by Means of Minimum Energy Principle. Soils and Foundations, 1992, 32(3): 97–116. DOI: 10.3208/sandf1972.32.3_97.

[7] Seid-Karbasi M, Hawson H, Atukorala U. Seismic stability of a Peruvian tailings earth-rockfill dam with liquefiable foundation. International Symposium on "Dams and Reservoirs under Changing Challenges" Held during the 79th Annual Meeting of the International Commission on Large Dams, 2011, 23: 613–620.

[8] Debarghya C Deepankar. Seismic Stability and Liquefaction Analysis of Tailings Dam. DISASTER ADVANCES, 2012, 5(3): 15–25.

[9] Chakraborty D Choudhury. Pseudo-Static and Pseudo-Dynamic Stability Analysis of Tailings Dam Under Seismic Conditions, PROCEEDINGS OF THE NATIONAL ACADEMY OF SCIENCES INDIA SECTION A-PHYSICAL SCIENCES, 2013, 83(1): 63–71. DOI: 10.1007/s40010-013-0069-5.

[10] Srikrishnan S Porathur, JL, Agarwal H. Impact of earthquake on mining slopes—A numerical approach. Arabian Journal of Geosciences, 2014, 7(12): 5193–5208. DOI: 10.1007/s12517-013-1144-6.

[11] Xu B, Wang Y. Stability analysis of the Lingshan gold mine tailings dam under conditions of a raised dam height. Bulletin of Engineering Geology and the Environment, 2015, 74(1): 151–161. DOI: 10.1007/s10064-014-0602-z.

[12] Naeini M, Akhtarpour A. Numerical analysis of seismic stability of a high centerline tailings dam. Soil Dynamics and Earthquake Engineering, 2018, 107: 179–194. DOI: 10.1016/j.soildyn.2018.01.019.

[13] Kokusho. Energy-Based Newmark Method for earthquake-induced slope displacements. Soil Dynamics and Earthquake Engineering, 2019, 121: 121–134. DOI: 10.1016/j.soildyn.2019.02.027.

[14] Alonso E, Gens A, Lloret A, et al. Effect of rain infiltration on the stability of slopes, PROCEEDINGS OF THE FIRST INTERNATIONAL CONFERENCE ON UNSATURATED SOILS/UNSAT' 95/PARIS/FRANCE/6-8 SEPTEMBER, 1995, 1: 1-5. https://trid.trb.org/view/468433.

[15] Ochiai H, Okada Y, Furuya G, et al. A fluidized landslide on a natural slope by artificial rainfall. Landslides, 2004, 1(3): 211–219. DOI: 10.1007/s10346-004-0030-4.

[16] Noguchi S, Nik A R, Yusop Z, et al. Rainfall-runoff Responses and Roles of Soil Moisture Variations to the Response in Tropical Rain Forest, Bukit Tarek, Peninsular Malaysia. Journal of Forest Research, 1997, 2: 125–132. DOI: 10.1007/BF02348209.

[17] Muntohar A S, Liao H-J. Rainfall infiltration: Infinite slope model for landslides triggering by rainstorm. NATURAL HAZARDS, 2010, 54(3): 967–984. DOI: 10.1007/s11069-010-9518-5.

[18] Zandarín M, Oldecop L, Pacheco R L, et al. The role of capillary water in the stability of tailing dams, Engineering Geology, 2009, 105: 108. DOI: 10.1016/j.enggeo.2008.12.003.

[19] Ormann L, Zardari M A, Mattsson H, et al. Numerical analysis of strengthening by rockfill embankments on an upstream tailings dam. Canadian Geotechnical Journal, 2013, 50(4): 391–399. DOI: 10.1139/cgj-2012-0255.

[20] Ng C W W, Shi Q. A numerical investigation of the stability of unsaturated soil slopes subjected to transient seepage. Computers and Geotechnics, 1998, 22(1): 1–28. DOI: 10.1016/S0266-352X(97)00036-0.

[21] Wang G, Kang J, Du C, et al. Study on Tailings Dam Over-Topping Failure Model Test and Break Mechanism Under the Rainfall Condition. TEHNICKI VJESNIK-TECHNICAL GAZETTE, 2017, 24(6): 1897–1904. DOI: 10.17559/TV-20170619031221.

[22] Hamade T, Mitri H. Reliability-based approach to the geotechnical design of tailings dams. INTERNATIONAL JOURNAL OF MINING RECLAMATION AND ENVIRONMENT, 2013, 27(6): 377–392. DOI: 10.1080/17480930.2013.772698.

[23] Sun Y, Gu X, Xu X. Experimental Study on Hydraulic Erosion Characteristics of Ecological Slope of Tailings Reservoir under Rainfall. KSCE JOURNAL OF CIVIL ENGINEERING, 2021, 25(7): 2426–2436. DOI: 10.1007/s12205-021-0912-1.

[24] Liu Y, Wang J, Zhang Z, et al. Effect on Tailing Dam Stability of Rainfall Infiltration. Advanced Materials Research, 2013, 842: 777–781. DOI: 10.4028/www.scientific.net/AMR.842.777.
[25] Gui R, He G. The Effects of Internal Erosion on the Physical and Mechanical Properties of Tailings under Heavy Rainfall Infiltration. Applied Sciences, 2021, 11(20): 9496. DOI: 10.3390/app11209496.
[26] Jakka R S, Ramana G V, Datta. Seismic Slope Stability of Embankments Constructed with Pond Ash. Geotechnical and Geological Engineering, 2011, 29(5): 821–835. DOI: 10.1007/s10706-011-9419-8.
[27] Yumin Chen. FLAC/FLAC 3D Fundamentals and Engineering Examples (Second Edition). Beijing, 2013.